# Dynamically adjustable asymmetric transmission and polarization conversion for linearly polarized terahertz wave*

Tong Li(李彤)[1], Fang-Rong Hu(胡放荣)[1,†], Yi-Xian Qian(钱义先)[2], Jing Xiao(肖靖)[3], Long-Hui Zhang(张隆辉)[1], Wen-Tao Zhang(张文涛)[1], and Jia-Guang Han(韩家广)[1]

[1] *Guangxi Key Laboratory of Optoelectronic Information Processing, Guilin University of Electronic Technology, Guilin* 541004, *China*
[2] *Key Laboratory of Optical Information Detecting and Display Technology, Zhejiang Normal University, Jinhua* 321004, *China*
[3] *Air Force Logistics College, Xuzhou* 221000, *China*

(Received 18 July 2019; revised manuscript received 14 October 2019; accepted manuscript online 5 December 2019)

The asymmetric transmission (AT) and polarization conversion of terahertz (THz) wave play a vital role in future THz communication, spectrum, and information processing. Generally, it is very difficult and complicated to actively control the AT of electromagnetic (EM) wave by using traditional devices. Here, we theoretically demonstrate a stereo-metamaterial (stereo-MM) consisting of a layer of metal structure and a layer of phase transition structure with a polyimide spacer in between. The performance of the device is simulated by using the finite-integration-technology (FIT). The results show that the AT and polarization conversion of linearly polarized wave can be dynamically controlled in a range of 1.0 THz–1.6 THz when the conductivity $\sigma$ of vanadium dioxide ($VO_2$) is changed under the external stimulation. This study provides an example of actively controlling of the AT and polarization conversion of the EM wave.

**Keywords:** stereo-metamaterial (stereo-MM), asymmetric transmission (AT), polarization conversion, vanadium dioxide ($VO_2$)

**PACS:** 42.79.Ci, 81.05.Xj, 84.30.Vn **DOI:** 10.1088/1674-1056/ab5ef8

## 1. Introduction

THz polarizers are very important in many applications, such as THz imaging, sensing, and spectroscopy. For example, high performance THz polarization converters are essential in the study of chiral structure of DNA,[1] THz polarization imaging,[2] and the determination of molecular structure.[3] The traditional methods to manipulate the polarization of electromagnetic (EM) wave are mainly based on birefringence,[4] and the polarization rotation angle is directly proportional to the length of the EM wave passing through the birefringent crystal. These devices are usually too bulky to be integrated. In addition, the transmission of EM wave is usually reciprocal, and the conventional method to achieve non-reciprocal transmission must break through the Lorentz reciprocity condition.[5] Generally, the reciprocity of interaction between EM wave and substance can be broken by the static magnetization of magneto-optic materials,[6] graphene,[7] and other materials, and then the non-reciprocal transmission is achieved. Obviously, it is very difficult to be integrated into small-scaled communication systems because of the additional bias magnetic fields.

Metamaterials (MMs) are artificial materials consisting of periodic sub-wavelength structures, which have unique EM properties.[8–11] High performance EM device is vital to realizing the EM wave manipulation, such as polarizer,[12] filter,[13] optical switch,[14] sensor,[15] *etc*. Many studies indicate that it is a simple and effective method of using MMs to achieve the polarization conversion of EM wave. At present, the MMs' microstructures can be used to realize many high-performance THz polarization converters. Grady *et al.*[16] proposed an ultrathin, broadband, and a highly efficient THz polarization converter that can transform a linear polarization state into its orthogonal one. Zhang *et al.*[17] proposed a single-layered broadband reflective THz line-to-circular polarizer. This polarizer can convert a linearly polarized wave into circularly polarized wave, and its bandwidth is associated with geometric parameters. Polarization conversion is usually accompanied by the asymmetric transmission (AT), and transmission parameters are related to the propagation direction of the EM wave. Compared with non-reciprocal transmission, the AT in MM follows the reciprocity theorem. Fedotov *et al.*[18] first demonstrated the AT of circularly polarized wave in a planar fish scale structure. Inspired by stereochemistry, a new concept of nanophotonics, *i.e.*, stereo-MM,[19] was proposed. These stereo-MMs have the same composition, but their spatial arrangements are different and exhibit completely different physical properties. After that, many MMs' devices have been demonstrated to realize the AT of

*Project supported by the National Natural Science Foundation of China (Grant Nos. 11574059 and 61965005), the National Technology Major Special Project, China (Grant No. 2017ZX02101007-003), the Natural Science Foundation of Guangxi Zhuang Autonomous Region, China (Grant No. 2018GXNSFAA050043), and the Guangxi Special Expert Program and Innovation Project of Guangxi Graduate Education, China (Grant Nos. 2019YCXS088 and 2019YCXS094), and the Foundation from Guangxi Key Laboratory of Automatic Detection Technology and Instrument, China (Grant No. YQ16101).

†Corresponding author. E-mail: hufangrong@sina.com

 

linear-polarized wave,[20–23] circular-polarized wave,[24–26] or both.[27,28] However, few of them is suitable for the THz band. More importantly, they cannot dynamically control the AT of THz wave nor the polarization conversion of the THz wave. For actively controlled MM,[29] the response can be tuned by using an external stimulus. As a phase change material, $VO_2$ has a fast phase transition speed[30] and low insertion loss.[31] The conductivity $\sigma$ of $VO_2$ can be changed by the electrical,[32–34] light,[35,36] and heat[37–40] excitation, which is an ideal material for THz tunable device.

In this work, we propose a stereo-MM which can dynamically control the AT of linearly polarized THz wave and the polarization conversion of linearly polarized THz wave. The device consists of a layer of metal copper (Cu) structure and a layer of $VO_2$ structure with a polyimide spacer between them. By changing the conductivity $\sigma$ of $VO_2$, the AT and polarization conversion of the linearly polarized wave can be dynamically controlled in a range of 1.0 THz–1.6 THz.

## 2. Design

The unit cell of the device is shown in Fig. 1(a), a 200-nm-thick Cu structure (yellow) and $VO_2$ structure (brown) are separated by a 21-μm-thick dielectric spacer of polyimide. The incident THz wave propagates along the $z$ axis, and the electric vector $\boldsymbol{E}$ and the magnetic vector $\boldsymbol{H}$ are in the $y$ axis and $x$ axis, respectively. Two ports are denoted as F and B. As shown in Fig. 1(b), the period of the unit cell is $p = 48$ μm. If the Cu structure is rotated 90° anti-clockwise along the $z$ axis and then rotated 180° along the $y$ axis, it can overlap the $VO_2$ structure.

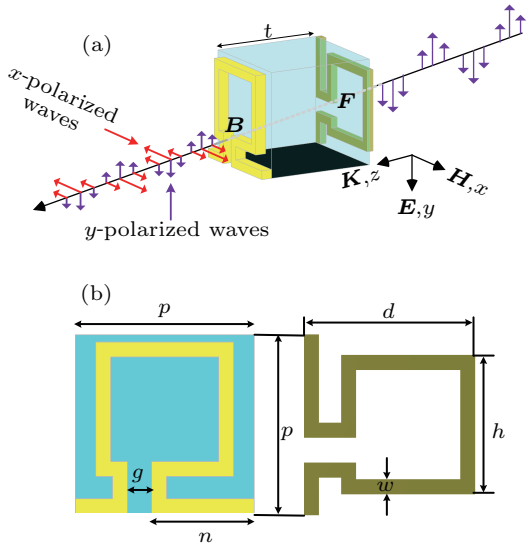


**Fig. 1.** Schematic diagram of the device, showing (a) perspective view, and (b) geometric parameters: $g = 6.5$ μm, $n = 27.5$ μm, $d = 46$ μm, $h = 36$ μm, $w = 4.0$ μm, and $t = 21$ μm.

In simulation, the Cu structure was taken as a lossy metal with conductivity of $5.96 \times 10^7$ S/m. Polyimide was modeled as a lossy dielectric with a dielectric constant $\varepsilon_{\text{polyimide}} = 2.4 + 0.005\text{i}$,[41] and the permittivity of $VO_2$ in the THz region is described by the Drude model as follows:[42]

$$\varepsilon(\omega) = \varepsilon_\infty - \frac{\omega_{\text{P}}^2(\sigma)}{\omega^2 + \text{i}\gamma\omega}, \tag{1}$$

where $\varepsilon_\infty = 12$ is the relative permittivity at high frequency, $\omega_p(\sigma)$ is the conductivity-dependent plasma frequency, $\gamma$ is the collision frequency and set to be $\gamma = 5.75 \times 10^{13}$ rad/s. In addition, both $\omega_{\text{p}}(\sigma)$ and $\sigma$ are proportional to free carrier density. The plasma frequency can be approximately expressed as

$$\omega_{\text{p}}^2(\sigma) = \frac{\sigma}{\sigma_{\text{ref}}}\omega_{\text{p}}^2(\sigma_{\text{ref}}), \tag{2}$$

where $\sigma_{\text{ref}} = 3.0 \times 10^5$ S/m, and $\omega_{\text{p}}(\sigma_{\text{ref}}) = 1.4 \times 10^{15}$ rad/s.

## 3. Basic concepts for AT

The unit cell (shown in Fig. 1(a)) of the device simultaneously loses mirror symmetry in the $z$ direction and 90° rotational symmetry in $x$–$y$ plane. Therefore, the chiral properties of the device can rotate the polarization direction of the EM wave. Assuming that the device lies in the $x$–$y$ plane, the incident and transmitted electric field in the $+z$ direction can be expressed as

$$\boldsymbol{E}_i(\boldsymbol{r},t) = \begin{pmatrix} I_x \\ I_y \end{pmatrix} \text{e}^{\text{i}(\kappa z - \omega t)}, \tag{3}$$

$$\boldsymbol{E}_t(\boldsymbol{r},t) = \begin{pmatrix} T_x \\ T_y \end{pmatrix} \text{e}^{\text{i}(\kappa z - \omega t)}, \tag{4}$$

where $I_x$ and $I_y$ are the complex amplitudes of the incident electric field in the $x$ and $y$ directions, $T_x$ and $T_y$ are the complex amplitudes of the transmitted field in the $x$ and $y$ directions, $\omega$ and $\kappa$ represent the frequency and wave vector, respectively.

For a linearly polarized wave, the relationship between the complex amplitude of the incident field and that of the transmitted field can be described by the Jones matrix[43]

$$\begin{pmatrix} T_x \\ T_y \end{pmatrix} = \begin{pmatrix} T_{xx} & T_{xy} \\ T_{yx} & T_{yy} \end{pmatrix} \begin{pmatrix} I_x \\ I_y \end{pmatrix} = T_{\text{lin}}^{\text{F}} \begin{pmatrix} I_x \\ I_y \end{pmatrix}, \tag{5}$$

where the meaning of four complex transmission coefficients are as follows: $T_{xx}$ means that both the incident wave and the transmitted wave are polarized in the $x$ direction; $T_{yy}$ denotes the incident wave and the transmitted wave both polarized in the $y$ direction; $T_{xy}$ refers to the incident wave and the transmitted wave polarized in the $y$ direction and the $x$ direction, respectively; $T_{yx}$ represents the incident wave and the transmitted wave both polarized in the $x$ direction and the $y$ direction, respectively. The subscript "lin" indicates the linear polarization, and the superscript "F" and "B" denote the forward and

backward propagations, respectively. According to the reciprocity theorem, the Jones matrix for the backward propagation direction can be described as

$$T_{\text{lin}}^{\text{B}} = \begin{pmatrix} T_{xx} & -T_{yx} \\ -T_{xy} & T_{yy} \end{pmatrix}. \quad (6)$$

In addition, the total transmission for the $y$-polarized wave along the forward direction and backward direction can be written as

$$t^{\text{F}} = t_{xy}^{\text{F}} + t_{yy}^{\text{F}}, \quad (7)$$

$$t^{\text{B}} = t_{xy}^{\text{B}} + t_{yy}^{\text{B}}, \quad (8)$$

where $t_{xy} = (T_{xy})^2$, and $t_{yy} = (T_{yy})^2$. For the linearly polarized wave, the AT parameter ($\Delta$) can be obtained from the Jones matrix

$$\Delta_{\text{lin}}^{(y)} = \left|T_{yy}^{\text{F}}\right|^2 + \left|T_{xy}^{\text{F}}\right|^2 - \left|T_{yy}^{\text{B}}\right|^2 - \left|T_{xy}^{\text{B}}\right|^2 = t^{\text{F}} - t^{\text{B}}, \quad (9)$$

$$\Delta_{\text{lin}}^{(x)} = \left|T_{xx}^{\text{F}}\right|^2 + \left|T_{yx}^{\text{F}}\right|^2 - \left|T_{xx}^{\text{B}}\right|^2 - \left|T_{yx}^{\text{B}}\right|^2 = -\Delta_{\text{lin}}^{(y)}, \quad (10)$$

where the superscript ($y$) and ($x$) indicate the $y$-polarized and the $x$-polarized wave, respectively.

## 4. Simulation and optical characterization

To investigate the influence of the conductivity $\sigma$ of $VO_2$ on the forward and backward propagations, the transmissions of $\sigma = 3.0 \times 10^2$ S/m and $\sigma = 5.0 \times 10^5$ S/m are calculated and the results are shown in Figs. 2(a) and 2(b), respectively.

As shown in Fig. 2(a), without the external stimulation, $VO_2$ is in insulator phase and has a very low conductivity, which is transparent for the THz wave.[31] The cross-polarized transmission $t_{xy}^{\text{F}} = t_{xy}^{\text{B}}$ and the co-polarized transmission $t_{yy}^{\text{F}} = t_{yy}^{\text{B}}$, which means that the transmission is symmetric. Under outer stimulation (see Fig. 2(b)), the $VO_2$ undergoes the insulator-to-metal transition. The cross-polarized transmission $t_{xy}^{\text{F}}$ is over 0.6 and $t_{xy}^{\text{B}}$ is below 0.05 in a range of 1.1 THz–1.4 THz, which indicates that the transmission is asymmetric. The results indicate that the proposed stereo-MM can realize the AT of linearly polarized wave by using the mode conversion.[20]

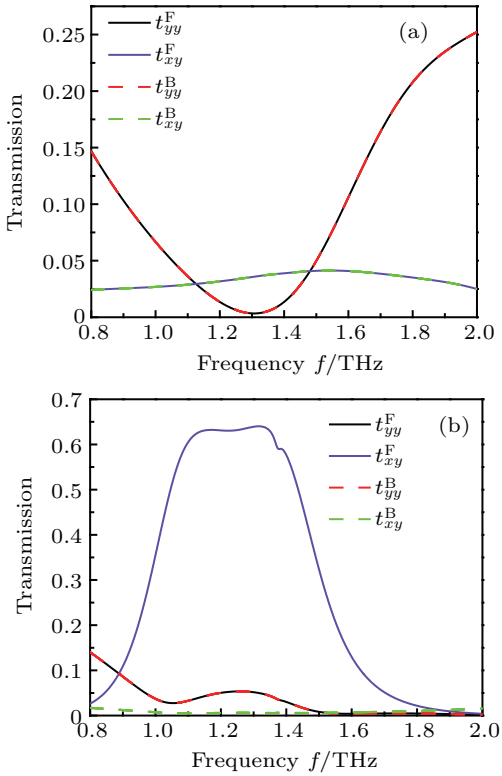


**Fig. 2.** Co-polarized and cross-polarized transmission of the forward and backward propagations under different $\sigma$ (a) $\sigma = 3.0 \times 10^2$ S/m and (b) $\sigma = 5.0 \times 10^5$ S/m.

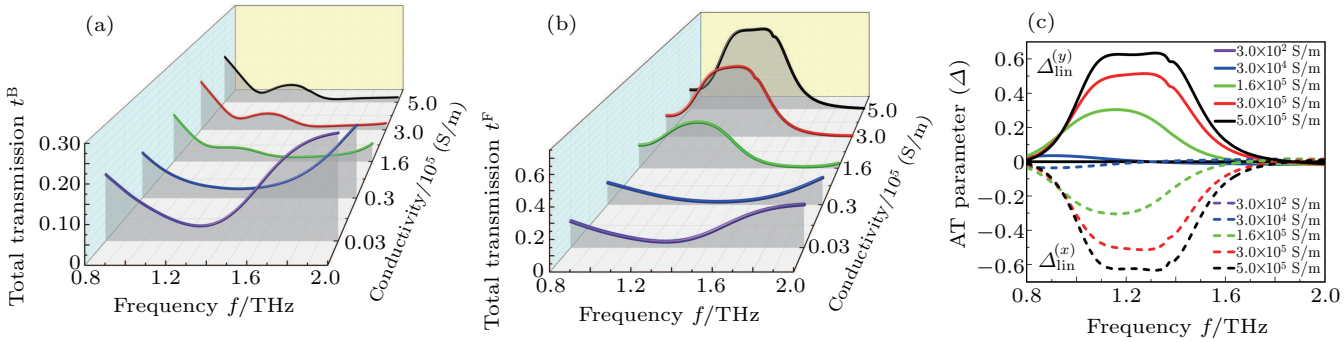


**Fig. 3.** Effects of conductivity $\sigma$ on total transmission and AT parameter for (a) backward propagation and (b) forward propagation, (c) AT parameters of $y$-polarized (solid line) and $x$-polarized waves (dashed line).

As shown in Fig. 3(a), the total transmission $t^{\text{B}}$ is very small in a range of 1.0 THz–1.5 THz. However, as shown in Fig. 3(b), the total transmission $t^{\text{F}}$ can be considerably improved by increasing the value of conductivity $\sigma$. The modulation depth (MD) of the total transmission $t^{\text{F}}$ is defined as

$$\text{MD} = \frac{t_{\text{max}}^{\text{F}} - t_{\text{min}}^{\text{F}}}{t_{\text{max}}^{\text{F}} + t_{\text{min}}^{\text{F}}}. \quad (11)$$

According to formula (11), the calculated MD can reach to 92.5% at 1.3 THz. In addition, as shown in Fig. 3(c), with the increase of conductivity $\sigma$, the AT parameter $\Delta_{\text{lin}}^{(y)}$ gradually increases from 0 to 0.63. Obviously, the transmission can be actively modulated by changing the value of conductivity $\sigma$.

Polarization conversion ratio (PCR) is another important parameter for evaluating the performance of the device, and it

can be calculated from the follow equation:

$$\mathrm{PCR} = \frac{|T_{xy}|^2}{|T_{xy}|^2 + |T_{yy}|^2} = \frac{t_{xy}}{t_{xy} + t_{yy}}. \tag{12}$$

When the conductivity $\sigma$ increases from $3.0 \times 10^2$ S/m to $5.0 \times 10^5$ S/m, the PCR of the forward propagation and the backward propagation are presented in Figs. 4(a) and 4(b), respectively.

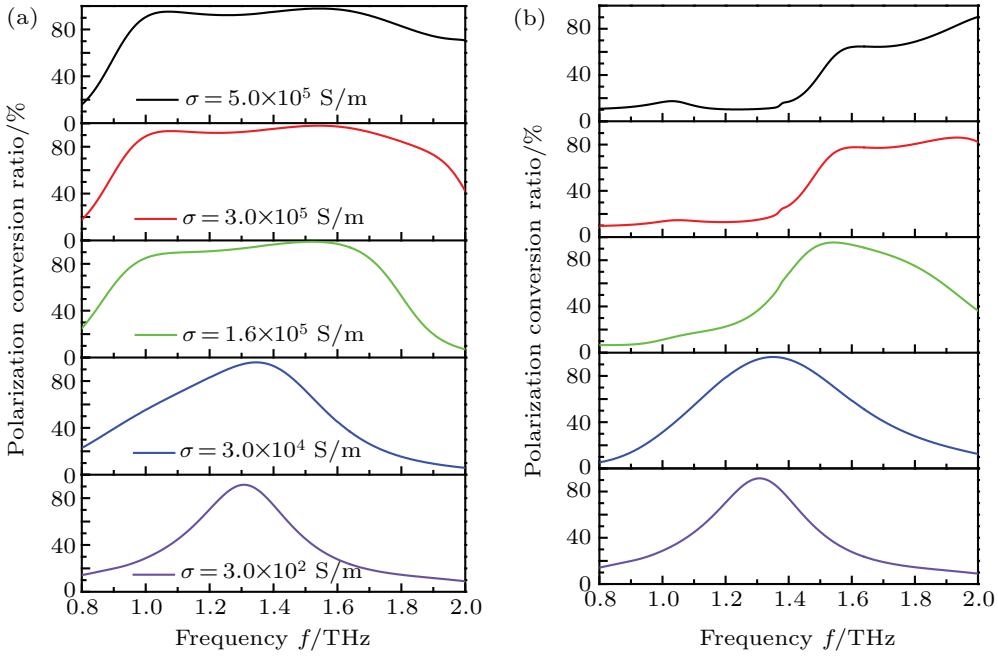


**Fig. 4.** Plots of PCR *versus* frequency at different values of conductivity $\sigma$ for (a) forward propagation and (b) backward propagation.

Figure 4(a) shows that for the forward propagation, the bandwidth of the PCR is significantly affected by the conductivity $\sigma$. When the conductivity of $VO_2$ is $5.0 \times 10^5$ S/m, the PCR is more than 90% in a range of 1.0 THz–1.6 THz. This indicates that the transmitted wave is mainly composed of the cross-polarized waves, but not the co-polarized waves. Figure 4(b) shows that for the backward propagation, the PCR decreases with conductivity $\sigma$ increasing in a range of 1.0 THz–1.4 THz. Obviously, the polarization conversion is suppressed. This indicates that when the same polarization wave propagates along different propagation directions, the difference in polarization conversion efficiency leads to the AT.

## 5. Physical mechanism

To understand physical mechanism of the AT and the polarization conversion for linearly polarized wave, the distributions of electric field at 1.2 THz are calculated and presented in Fig. 5.

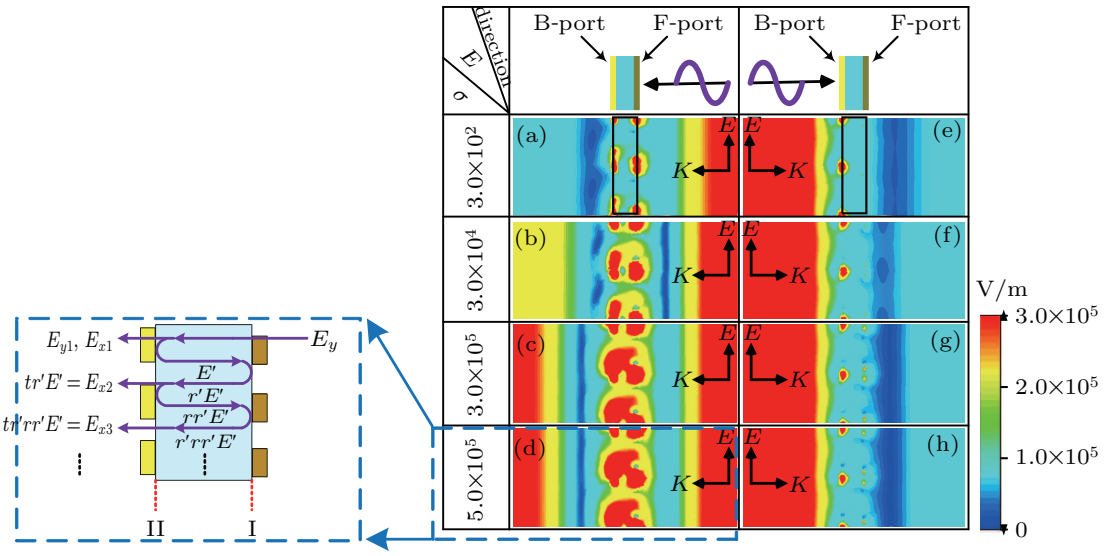


**Fig. 5.** Electric field distributions under different values of conductivity $\sigma$ (at 1.2 THz).

As shown in Figs. 5(a)–5(d), for the forward propagation, when the conductivity $\sigma$ increases from $3.0\times10^2$ S/m to $5.0\times10^5$ S/m, the internal and left electric field of the device are gradually enhanced. For example, figure 5(d) indicates that the electric fields are almost symmetrically distributed on both sides of the device when $\sigma = 5.0\times10^5$ S/m, which can be explained by using the Fabry–Perot resonance of a multilayer structure[44,45] as indicated in the left inset of Fig. 5. The symbol "I" represents the interface between the polyimide and the $VO_2$ structure, and "II" denotes the interface between the polyimide and the Cu structure layer. Parameters $r'$ represents the reflection coefficient of the $x$-polarized wave at I, and $t$ and $r$ denote the transmission coefficient and reflection coefficient of the $x$-polarized wave at II, respectively. Because the $VO_2$ (see in Fig. 5) is in the metallic phase, it can form a resonant cavity with the Cu structure, and thus increasing the total transmission.

Meanwhile, figures 5(e)–5(h) show that for the backward propagation, the conductivity $\sigma$ has little effect on the electric field distribution inside and on the right of the device. The probable reason is that the y-polarized incident wave is almost reflected by the Cu structure.

In addition, to understand in depth the physical mechanism of the AT and the polarization conversion for linearly polarized wave, the distributions of surface current under the different values of conductivity $\sigma$ (at 1.2 THz) are shown in Fig. 6.

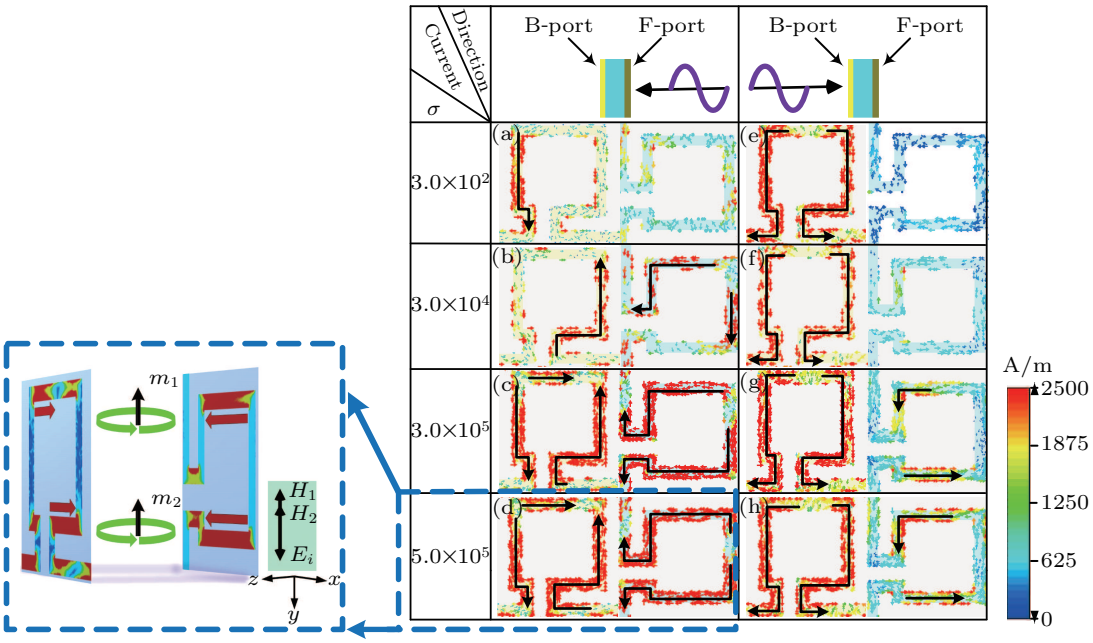


**Fig. 6.** Surface current distributions under different values of conductivity $\sigma$ (at 1.2 THz).

For the forward propagation, the surface currents on the surface of the Cu structure and that on the $VO_2$ structure are presented in Figs. 6(a)–6(d). It is evident that the surface currents on both sides are generated by two electrical dipoles, and the surface currents become strong and dense with the increase of $\sigma$ value. Meanwhile, figures 6(e)–6(h) show the surface current distributions of the backward propagation. They are produced by two dipoles oscillating on the surface of the Cu structure, and only few currents are distributed on the surface of the $VO_2$ structure.

The polarization conversion of $y$-polarized incident wave mainly results from the magnetic response between surface currents. The left inset of Fig. 6 shows the distribution of surface current along the $x$ direction. In this inset, the red arrow represents the direction of current. Obviously, the current direction on the Cu structure is opposite to that on the $VO_2$ structure, and thus forming two current loops of the same shape (shown as green), generating two magnetic dipoles $m_1$ and $m_2$, and correspondingly inducing two magnetic fields $\boldsymbol{H}_1$ and $\boldsymbol{H}_2$. Due to the $\boldsymbol{H}_1$ and $\boldsymbol{H}_2$ being parallel to the direction of the incident electric field $\boldsymbol{E}_\mathrm{i}$, the cross-coupling between the induced magnetic fields $\boldsymbol{H}_1$ and $\boldsymbol{H}_2$ and the incident electric field $\boldsymbol{E}_\mathrm{i}$ results in the change of polarization direction.[26,46]

## 6. Conclusions and perspectives

In this work, by using the insulator-to-metal transition of $VO_2$, a stereo-MM which can be used to dynamically control the AT and polarization conversion of linearly polarized wave in the THz band is proposed. By actively changing the $\sigma$ of $VO_2$ structure, the dynamically adjustable AT and polarization conversion of the linearly polarized wave is theoretically demonstrated ina range of 1.0 THz–1.6 THz. The proposed stereo-MM is easy to modulate and integrate, and also has many advantages, such as diverse modulation modes, fast

response, *etc*. These characteristics can be widely applied to THz communication, information processing, integrated optics, and other fields. This study provides a simple and feasible approach to achieving the dynamically adjustable AT and polarization conversion of the THz wave.

## References


[1] Brucherseifer M, Nagel M, Haring Bolivar P, Kurz H, Bosserhoff A and Büttner R 2000 *Appl. Phys. Lett.* **77** 4049

[2] Zhang L L, Zhong H, Deng C, Zhang C L and Zhao Y J 2011 *Opt. Commun.* **284** 4356

[3] Chen H L, Bian H T, Li J B, Guo X M, Wen X W and Zheng J R 2013 *J. Phys. Chem. B* **117** 15614

[4] Wiesauer K and Christian Jördens 2013 *J. Infrared Milli Terahz Waves* **34** 663

[5] Jalas D, Petrov A, Eich M, Freude W, Fan S, Yu Z, Baets R, Popvić M, Melloni A, Joannopoulos J D, Vanwolleghem M, Doerr C R and Renner H 2013 *Nat. Photon.* **7** 579

[6] Wang H, Wu H and Zhou J Q 2018 *J. Quant. Spectrosc. & Radiat. Transfer* **206** 254

[7] Tamagnone M, Moldovan C, Poumirol J M, Kuzmenko A B, Ionescu A M, Mosig J R and Perruisseau J 2016 *Nat. Commun.* **7** 11216

[8] He X Y, Chen Q, Li L C, Yang C, Li B, Zhou B H and Tang C X 2011 *Chin. Phys. Lett.* **28** 057701

[9] Chen L, Wei Y M, Zang X F, Zhu Y M and Zhuang S L 2016 *Sci. Rep.* **6** 22027

[10] Liu C J, Huang Y Y, Yao Z H, Yu L L, Jin Y P and Xu X L 2018 *Europhys. Lett.* **121** 44004

[11] Wang J F, Qu S B, Xu Z, Xia S, Ma H, Wang Q, Yang Y M and Wu X 2010 *Chin. Phys. Lett.* **27** 034104

[12] Zhang X J, Wu X and Xu Y D 2017 *Chin. Phys. Lett.* **34** 084102

[13] Hu F R, Xu X, Li P, Xu X L and Wang Y E 2017 *Chin. Phys. B* **26** 074219

[14] Liu J Q, Chen J, Wuan D Y, Zhou Y X, Chen Z H and Wang L L 2013 *Chin. Phys. Lett.* **30** 097801

[15] Xia W 2013 *Chin. Phys. Lett.* **30** 077308

[16] Grady N K, Heyes J E, Chowdhury D R, Zeng Y, Reiten M T, Azad A K, Taylor A J, Dalvit D A R and Chen H T 2013 *Science* **340** 1304

[17] Zang X F, Liu S J, Gong H H, Wang Y J and Zhu Y M 2018 *J. Opt. Soc. Am. B* **35** 950

[18] Fedotov V A, Mladyonov P L, Prosvirnin S L, Rogacheva A V, Chen Y and Zheludev N I 2006 *Phys. Rev. Lett.* **97** 167401

[19] Liu N, Liu H, Zhu S N and Giessen H 2009 *Nat. Photon.* **3** 157

[20] Kim M, Yao K, Yoon G, Kim I, Liu Y and Rho J 2017 *Adv. Opt. Mater.* **5** 1700600

[21] Mutlu M, Akosman A E, Serebryannikov A E and Ozbay E 2011 *Opt. Express* **19** 14290

[22] Zhou X, Li M H, Wang H B, Wang C, Zhai X M and Dong J F 2017 *J. Electromagn. Waves Applications* **31** 828

[23] Li Z C, Chen S Q, Tang C C, Liu W W, Cheng H, Liu Z, Li J X, Yu P, Xie B Y, Liu Z C, Li J J and Tian J G 2014 *Appl. Phys. Lett.* **105** 201103

[24] Tang D F, Wang C, Pan W K, Li M H and Dong J F 2017 *Opt. Express* **25** 11329

[25] Bai Y, Chen Y Y, Zhang Y Y, Wang Y K, Aba T, Li H, Wang L and Zhang Z Y 2018 *J. Phys.: Condebsed Matter* **30** 114001

[26] Liu D J, Xiao Z Y, Ma X L and Wang Z H 2015 *Appl. Phys. Express* **8** 52001

[27] Plum E, Fedotov V A and Zheludev N I 2009 *Appl. Phys. Lett.* **94** 131901

[28] Cheng Z Z and Cheng Y Z 2019 *Opt. Commun.* **435** 178

[29] Hashemi M R, Cakmakyapan S and Jarrahi M 2017 *Rep. Prog. Phys.* **80** 094501

[30] Nakajima M, Takubo N, Hiroi Z, Ueda Y and Suemoto T 2008 *Appl. Phys. Lett.* **92** 011907

[31] Shi Q W, Huang W X, Zhang Y X, Yan J Z, Zhang Y B, Mao M, Zhang Y and Tu M J 2011 *ACS Appl. Mater. Interfaces* **3** 3523

[32] Han C R, Parrott E P J, Humbert G, Crunteanu A and Pickwell-macpherson E 2017 *Sci. Rep.* **7** 12725

[33] Ruzmetov D, Gopalakrishnan G, Ko C, Narayanamurti V and Ramanathan S 2010 *J. Appl. Phys.* **107** 114516

[34] Liu M K, Hwang H, Tao H, Strikwerda A C, Fan K, Keiser G R, Sternbach A J, West K G, Kittiwatanakul S, Lu J W, Wolf S A, Omenetto F G, Zhang X, Nelson K A and Averitt R D 2012 *Nature* **487** 345

[35] Wan C H, Horak E H, King J, Salman J, Zhang Z, Zhou Y, Roney P, Gundlach B, Ramanathan S, Goldsmith R H and Kats M A 2018 *ACS Photon.* **5** 2688

[36] Zhang C H, Zhou G H, Wu J B, Tang Y H, Wen Q Y, Li S X, Han J G, Jin B B, Chen J and Wu P H 2019 *Phys. Rev. Appl.* **11** 054016

[37] Karaoglan-Bebek G, Hoque M N F, Holtz M, Fan Z and Bernussi A A 2014 *Appl. Phys. Lett.* **105** 201902

[38] West K G, Lu J W, Yu J N, Kirkwood D, Chen W, Pei Y H, Claassen J and Wolf S A 2008 *J. Vac. Sci. Technol. A* **26** 133

[39] Wen Q Y, Zhang H W, Yang Q H, Xie Y S, Chen K and Liu Y L 2010 *Appl. Phys. Lett.* **97** 021111

[40] Wang D C, Zhang L C, Gu Y H, Mehmood M Q, Gong Y D, Srivastava A, Jian L K, Venkatesan T, Qiu C W and Hong M H 2015 *Sci. Rep.* **5** 15020

[41] Ma Y, Chen Q, Grant J, Saha S C, Khalid A and Cumming D R S 2011 *Opt. Lett.* **36** 945

[42] Wang S X, Kang L and Werner D H 2018 *Sci. Rep.* **8** 189

[43] Menzel C, Rockstuhl C and Lederer F 2010 *Phys. Rev. A* **82** 53811

[44] Li J H, Guo H J, Xu T, Chen L, Hang Z H, Zhou L and Chen S Q 2019 *Phys. Rev. Appl.* **11** 044042

[45] Cheng Y Z, Fan J P, Luo H, Feng N X, Mao X S and Gong R Z 2019 *Opt. Mater. Express* **9** 1365

[46] Huang X J, Yang D, Yu S Q, Guo L, Guo L Y and Yang H L 2014 *Appl. Phys. B* **117** 633